Delalieux, S.; Zarco-Tejada, PJ.; Tits, L.; Jiménez Bello, MA.; Intrigliolo Molina, DS.; Somers, B. (2014). Unmixing-Based Fusion of Hyperspatial and Hyperspectral Airborne Imagery for Early Detection of Vegetation Stress. IEEE Journal of Selected Topics in Applied Earth Observations and Remote Sensing. 7(6):2571-2582. doi:10.1109/JSTARS.2014.2330352.

Draft

Unmixing based fusion of remotely piloted aircraft systems and airborne hyperspectral imagery for early detection of vegetation stress

Delalieux S.[1], Zarco-Tejada, P.J.[2], Tits, L[3], Somers, B.[1]

[1]Flemish Institute for Technological Research, Boeretang 200, 2400 Mol, Belgium, Stephanie.Delalieux@vito.be, Telephone + 32 (0) 14 33 67 16 Fax + 32 14 32 2795

[2]IAS-CSIC Quantalab

[3] Dept. of Biosystems, M3-BIORES, Katholieke Universiteit Leuven, W. de Croylaan 34, BE- 3001 Leuven, Belgium

Keywords – thermal, citrus, hyperspectral and hyperspatial fusion, water stress

ABSTRACT

Current satellite remote sensing instruments still face a trade-off between spectral and spatial resolution. Moreover, for many applications the timely acquisition of satellite remote sensing data is expensive and often not achievable. This gap between information needs and data availability inspires research on using Remotely Piloted Aircraft Systems (RPAS) to capture the desired high spectral and spatial information, furthermore providing temporal flexibility. Present full-range hyperspectral sensors are yet not suited to be operated on RPAS systems, due to sensor weight and instability. This motivated the investigation of an unmixing based data fusion approach to combine available airborne hyperspectral (APEX) and hyperspatial (RPAS) sensor imagery. As such, the fused dataset provides huge potential for more in-depth spectral and spatial analysis. This manuscript looks into the use of a hyperspectral-hyperspatial fusion technique for better biophysical parameter retrieval and physiological assessment in agricultural crops. To confirm this statement, a biophysical parameter extraction study was performed on a simulated citrus orchard using a 3D radiative transfer approach. Furthermore, the unmixing based fusion was applied on a real test case in commercial citrus orchards with discontinuous canopies, in which a more efficient and accurate estimation of water stress was achieved by fusing thermal RPAS and hyperspectral APEX imagery. Narrow-band reflectance indices

that have proven their effectiveness as pre-visual indicators of water stress, such as the Photochemical Reflectance Index (PRI), showed a significant increase in tree water status detection accuracy when applied on the fused dataset compared to the original hyperspectral APEX dataset (R^2=0.62 vs R^2=0.21). This approach could be extended globally for the fusion of high spatial and high spectral resolution satellite imagery, enabling also a temporal hyperspectral, hyperspatial analysis.

1. INTRODUCTION

Due to physical limitations and data-transfer requirements the design and development of remote sensors face a trade-off between (i) the signal-to-noise ratio, (ii) the spatial, and (iii) spectral resolution. The Hyperion sensor on board EO-1 satellite currently offers the highest spectral resolution available from space. The spatial resolution of only 30 meters however restricts a proper use of the inherent potential of these data for detailed mapping purposes and precision farming applications. On the other hand, sensors such as Quickbird and WorldView-2 are able to offer very high spatial resolution imagery, but at the expense of their spectral resolution: panchromatic at sub-meter spatial resolution, and 4 to 8 broad spectral bands (Worldview-2) with approximately 2.5 m spatial resolution. With the launch of new very high resolution satellites such as Worldview-3 and planned hyperspectral missions like Enmap, Prisma and Hyspiri much more data will become available to the user community. Still, the trade-off in spectral and spatial resolution will remain and new advanced data and decision fusion approaches are needed to make optimal use of the future sensor ensembles.

On a different scale, hyperspectral airborne sensors such as APEX (Airborne Prism EXperiment), AHS (Airborne Hyperspectral Scanner), CASI (Compact Airborne Spectrographic Imager), AVIRIS (Airborne Visible/Infrared Imaging Spectrometer), and Hymap (Hyperspectral Mapper), also have to deal with this

spectral-spatial resolution trade-off. These hyperspectral airborne systems are limited to a spatial resolution of around 2m, which for specific applications might not sufficient. This is especially true for many precision farming applications in which the retrieval of spatial and spectral variability within heterogeneous orchards is of great importance for identifying crop stress that is one of the major factors influencing farming management decisions making. Suarez et al. (2010), for example, indicated the importance of acquiring very high spatial resolution imagery (~ 0.2m) for assessing fruit quality and water stress in citrus and olive orchards using airborne Photochemical Reflectance Index (PRI) formulation. Stuckens et al. (2010) came to a similar conclusion when exploring the amount of spectrally mixed pixels (i.e. trees, weeds and/or soil all occur within a single image pixel) in simulated orchards. They concluded that pixel sizes should be smaller than 1 m in order to obtain a minimum of 50 percent pure pixels and smaller than 10 cm for 82 percent pure pixels. Follow-up studies demonstrated that these mixing effects of plants and background/litter, whether linear or non-linear, play an important role in obstructing a detailed assessment of crop conditions in these heterogeneous architectures (Tits et al., 2012, 2013). For these reasons, Guo et al., (2012) suggested that RPAS remote sensing is very valuable for the applications of precision agriculture and to generate quantitative mapping products.

Innovative developments in RPAS platforms and associated sensing technologies are nowadays expanding at an increasing rate, bringing image resolutions to unprecedented levels of detail, thereby opening exciting new application opportunities (Berni et al., 2009). This is especially of huge interest to the precision farming community which requires flexible and frequent data capturing. Though, mainly due to payload restrictions, full-range optical hyperspectral sensors (i.e., ranging from 350 – 2500 nm) are not yet suited to be operated in an operational manner on these lightweight RPAS platforms proposed for precision agriculture. To our

knowledge, only few studies have successfully tested pushbroom hyperspectral VNIR sensors on a small, lightweight, fixed-wing RPAS (Zarco-Tejada et al., 2012; 2013).

In an attempt to overcome current spatial-spectral resolution tradeoffs in spectral sensor design, this study investigates the possibility of assembling a promising new data source through fusing very-high spatial and high spectral imagery based on unmixing techniques, as such enabling more detailed monitoring purposes. We thereby hypothesize that the combination of the high spatial resolution imagery captured by a RPAS and the more detailed spectral information available from airborne hyperspectral sensors, albeit at lower spatial resolution, can help to overcome the spatial-spectral data availability trade-off. Such a fusion technique was previously proposed by Zurita-Milla et al. (2008), who extended on the work of Zhukov (1999) and Filiberti (2005). In each of these studies, a multi-sensor, multi-resolution fusion technique was applied to unmix low-resolution images using the information about their pixel composition from co-registered high-resolution images. Yet, none of these studies were performed on very high spatial (cm resolution) and hyperspectral datasets. Filiberti (2005) merged a high-spatial-resolution panchromatic band with a low-spatial-resolution multispectral Landsat TM band with a 1:2 ground sample distance (GSD) ratio between the panchromatic (15-m) and the TM multispectral band (30-m). As such, he aimed at restoring the multispectral image using content from the higher resolution panchromatic image. Zurita-Milla et al. (2008) showed that the unmixing based data fusion approach can be used to successfully downscale MERIS FR information (300 m pixel size, 15 bands) to a Landsat-like spatial resolution (25 m pixel size, 6 bands) and as such obtain better MERIS land products. They successfully used the MERIS fused images to assess vegetation status by evaluating the Normalized Difference Vegetation Index (NDVI), the Modified Transformed Chlorophyll Index (MTCI) and the Modified Green Vegetation Index (MGVI).

In this study, the added value of the unmixing based fusion of unmanned aerial systems and airborne hyperspectral imagery is investigated in light of pre-visual estimation of crop stress in commercial citrus orchards characterized by a discontinuous canopy. The spatial unmixing fusion algorithm is therefore implemented and applied on simulated and in-situ high spatial and high spectral citrus orchard image data sets. The simulated citrus orchard thereby serves as a preliminary validation tool for the fusion algorithm. For the in-situ datasets, the fusion process is applied on the most detailed information available both spectrally and spatially. Hyperspatial (cm) images are gathered by a highly flexible RPAS, while the hyperspectral data was acquired by the APEX sensor. The fused or spatially unmixed (SpU) hyperspectral – hyperspatial dataset allowed us to assess the performance of narrow-band physiological indices for estimating stress levels in citrus orchards at a 20 cm scale.

1. THEORETICAL BACKGROUND

1.1 Spectral Unmixing method

Spectral unmixing or spectral mixture analysis (SMA) is a commonly used image analysis technique converting mixed pixel reflectance values into numerical sub-pixel fractions of a few ground components (Adams & Gillespie, 2006). Although nonlinear mixing effects are well-acknowledged in vegetated areas (Roberts, 1991; Borel & Gerstl, 1994; Somers et al., 2009), mixed pixel signals (r) are generally modeled as a linear combination of pure spectral signatures of its constituent components (i.e., endmembers), weighted by their subpixel fractional cover (Adams et al., 1986):

$$r = Mf + \varepsilon \quad (1)$$

115 In Eq. (1) M is a matrix in which each column corresponds to the spectral signal of a specific endmember. f is
116 a column vector $[f1,\ldots,fm]^T$ denoting the cover fractions occupied by each of the m endmembers in the pixel.
117 ε is the portion of the spectrum that cannot be modeled using these endmembers.
118
119 Critical to successful SMA is the selection of appropriate endmembers (Elmore et al., 2000; Tompkins et al.,
120 1997). The spectral signatures of the endmembers may be (i) derived from spectral libraries built from field
121 or laboratory measurements, obtained using ground based or portable spectro-radiometers (e.g., Asner &
122 Lobell, 2000; Roberts et al., 1998); (ii) derived directly from the image data themselves (e.g., Bateson et al.,
123 2000; Plaza et al., 2002; Somers et al., 2012); or (iii) simulated using radiative transfer models (e.g., Peddle
124 et al., 1999; Painter et al., 2003; Tits et al., 2012).
125
126 Once the endmembers and their spectral signatures are known and if the number of endmembers is less than
127 the number of spectral bands, the system of equations in (1) is over-determined and may uniquely be inverted
128 using techniques to solve for the fractions with minimal additional error in the equations. Least squares
129 regression analysis is one of the most commonly used optimization techniques (Barducci & Mecocci, 2005).
130 SMA can be implemented without constrains (e.g., Harsayni & Chang, 1994), but physically meaningful
131 abundance estimates are often obtained by constraining the coefficients in (1) to sum to unity and to be
132 positive (Adams et al., 1993).
133
134 1.2 Spatial Unmixing
135 Spatial unmixing is an image fusion technique which aims at combining the detailed information from two
136 images over the same study area: one with low spatial and high spectral resolution (in our case a
137 hyperspectral airborne image), and one with high spatial and low spectral resolution (in our case an RPAS

image). Spatial unmixing differs from spectral unmixing as it tries to recover the material spectra for classes within a pixel, instead of the cover fractions of the different materials. The material fractions can be deduced from the high spatial, low spectral resolution RPAS image. Figure 1 gives a visual representation of the spatial unmixing technique. Several steps are involved in the procedure starting with the classification of the high spatial resolution image in *n* classes (*in casu*, soil and vegetation). Fraction maps, *F*, are subsequently created per pre-defined kernel *k* (*in casu*, five by five) of the hyperspectral pixels, by counting for each class the amount of high resolution pixels which are present in the corresponding lower resolution pixel. Once the fraction maps *F* are calculated and given the hyperspectral reflectance values for the hyperspectral pixels *R* at a particular wavelength of interest, the spatial unmixing equation can be solved by least squares optimization, in order to find the reflectance value at that particular wavelength of the class endmembers, *M*. The unmixing is thus solved for each low resolution band independently. Therefore, a kernel size larger than or equal to the number of classes present in the neighbourhood had to be chosen, because each hyperspectral pixel provides only one mixing equation (Zurita-Milla, 2008). Finally, each of the *n* classes present in the central pixel of the neighborhood is replaced by its corresponding unmixed signal. By repeating this operation for all the airborne hyperspectral pixels, and bands and for different combinations of *n* and *k*, a series of fused images is generated in which endmember variability is induced, which can be seen as a major benefit of this unmixing based fusion method.

Analogous to equation 1, the unmixing based fusion method can be defined as follows

$$R^{i,k} = M^{i,k,n} \cdot F^{k,m} + \varepsilon \qquad (2)$$

In (2) $R^{i,k}$ is a vector that contains the values of band *i* for all the hyperspectral pixels present in the neighborhood *k*. $M^{i,k,n}$ is the unknown vector containing spectral information of each of the classes present in *k*. $F^{k,n}$ is a matrix containing the cover fractions occupied by each of the *m* endmembers in each pixel in *k*. ε is the portion of the spectrum that cannot be modeled.

This indirectly implies that the number of classes (*n*) and the size of the neighborhood (*k*) need to be optimized. *n* needs to be optimized based on the application demand and on the spectral variability of the scene. *k* also needs to be optimized because it has a great impact on the spectral quality of the fused image.

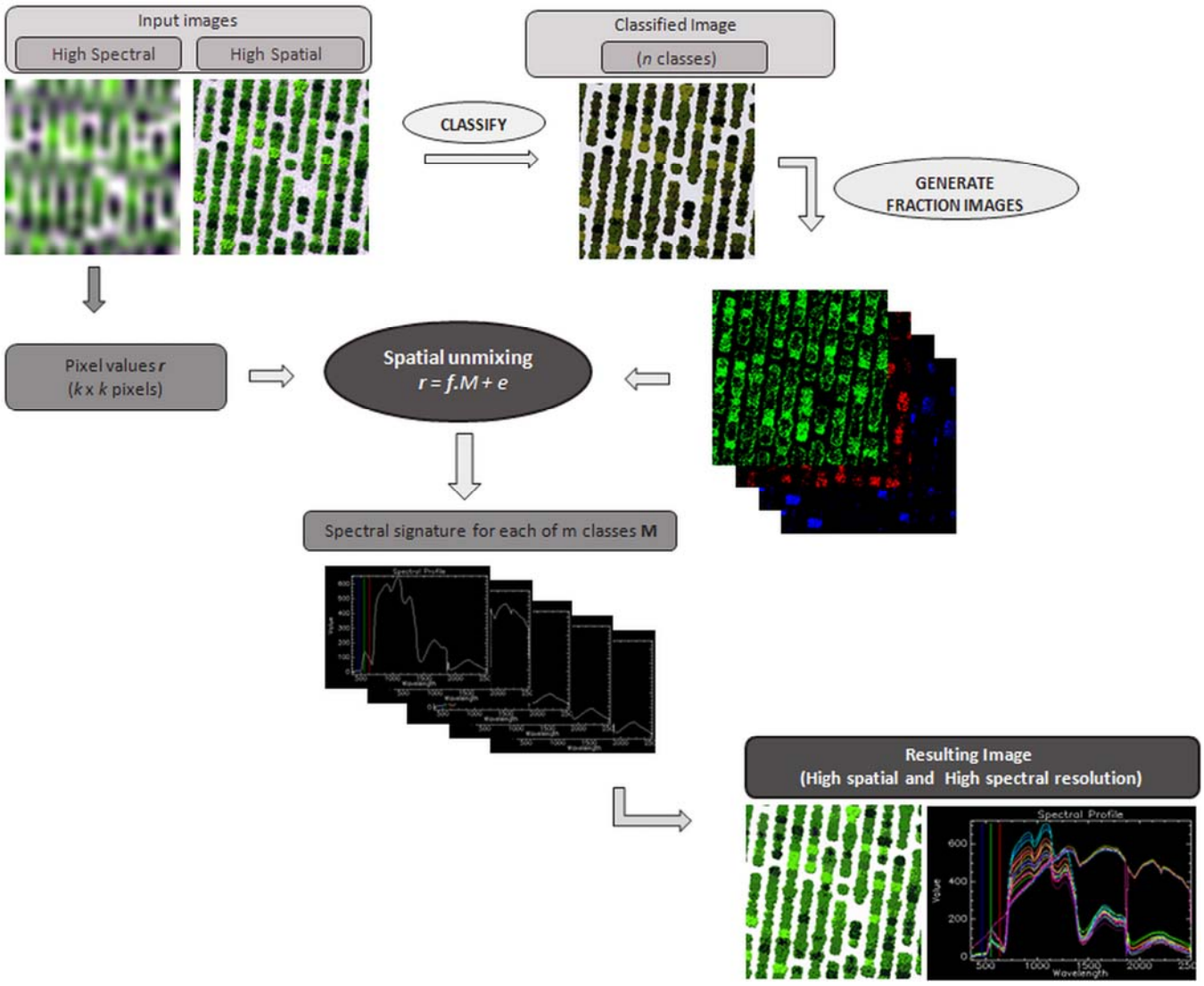

Figure 1. Overview of the spatial unmixing technique

169

170 ## 2. MATERIALS AND METHODS

171 ### 2.1 Simulated dataset

172 For this study a ray-tracing experiment in a fully calibrated virtual 3D representation of a citrus orchard was
173 used. This 3D radiative transfer model has been integrated in the web-based RAMI Online Model Checker
174 (ROMC) service (Widlowski et al., 2008, and has previously been used as a reference tool for validation of
175 image analysis techniques for precision farming (e.g., Tits et al., 2012b; Tits et al., 2013). Based on detailed
176 in situ calibration measurements, virtual 3D replicas of orchard trees were built as triangular meshes using an
177 implementation tree geometry algorithm developed in Weber and Penn (1995) (Figure 2). All reference data
178 for calibration (and validation) was collected in a 9-year-old Valencia 'Midknight' orange grove near
179 Wellington, South Africa (33°13'60''S; 18°15'60''E, altitude 100 m). The orchard block had a row spacing
180 of 4.5 m, a tree spacing of 2 m and a row azimuth of 7.3°. For each tree, tree vigour (i.e, LAI, height, crown
181 width and diameter) and optical properties (leaf and canopy reflectance) were determined. Canopy and leaf
182 reflectance spectra were collected using an ASD FR spectroradiometer (Analytical Spectral Devices,
183 Boulder, CO) ranging from 350 to 2500 nm with a spectral resolution of 3 nm in the VIS and NIR and 10 nm
184 in the SWIR. A 25° field of view (FOV) bare fiber optic was used. Within the orchard, 60 trees were selected
185 that span the range of structural and spectral variability encountered in the orchard. Leaf chlorophyll and
186 water content were derived from the measured leaf spectra through inversion of the PROSPECT model
187 (Jacquemoud and Baret, 1990). These field measurements were used to calibrate 3D replicas of the measured
188 trees. In order to increase the observed variability in tree conditions we further created for each of the 3D
189 trees three additional clones. While the overall tree architecture remained the same, we created (i) one clone
190 with similar leaf spectra but with a LAI which was 56% of the reference trees by randomly removing part of
191 the leaves, (ii) one clone with similar LAI and leaf water content but reduced leaf chlorophyll content (50%

of the reference chlorophyll) (note that the new reflectance coefficients were recalculated with the PROSPECT model (Stuckens et al., 2009)), (iii) one clone with similar LAI and leaf chlorophyll but reduced water content (70% of reference). The new reflectance coefficients were recalculated with the PROSPECT model (Stuckens et al., 2009). Thus extra variability in the biophysical parameters and the spectral data was created to incorporate different types of stress. All 3D tree replicas were then randomly placed in the orchard. The physical and optical properties of the soil (sandy texture, gravimetric moisture content ranging between 0 and 15%) were determined and used to the virtual model. Full details on the calibration procedure can be found in Stuckens et al. (2009) while a more detailed description of the field campaign can be found in Somers et al. (2009).

Three synthetic images of the virtual orchard were generated using a modified version of a physically based ray-tracer (Pharr & Humphreys, 2004) (Figure 3). The first image of 400 by 400 pixels provided information in 216 spectral bands ranging from 350 to 2500 nm with a spectral resolution of 10 nm and a spatial resolution of 2 m (referred to as LR-HS, left panel of Figure 3). This is similar to what nowadays can be delivered by airborne hyperspectral sensors. A RGB representation of the image scene is shown in the right panel of Figure 3. The second scene, depicted in the centre panel of Figure 3, simulated an image captured by a RGB sensor onboard an RPAS. The image of 4000 by 4000 pixels with a spatial resolution of 0.2 m is further referred to as HR) (Figure 3, centre panel).

The third or reference image scene simulated a 216 band hyperspectral sensor ranging from 350 to 2500 nm with a spectral resolution of 10 nm and a spatial resolution of 0.20 m (HR-HS). Such detailed imagery is currently not yet achievable by airborne or satellite systems but serves as a perfect reference scene to test the

efficiency of the unmixing based data fusion of the first two image scenes. For each simulated image scene detailed fraction images were available.

Figure 2: (left) A virtual 3D replica of an orchard tree, (right) a real orchard tree

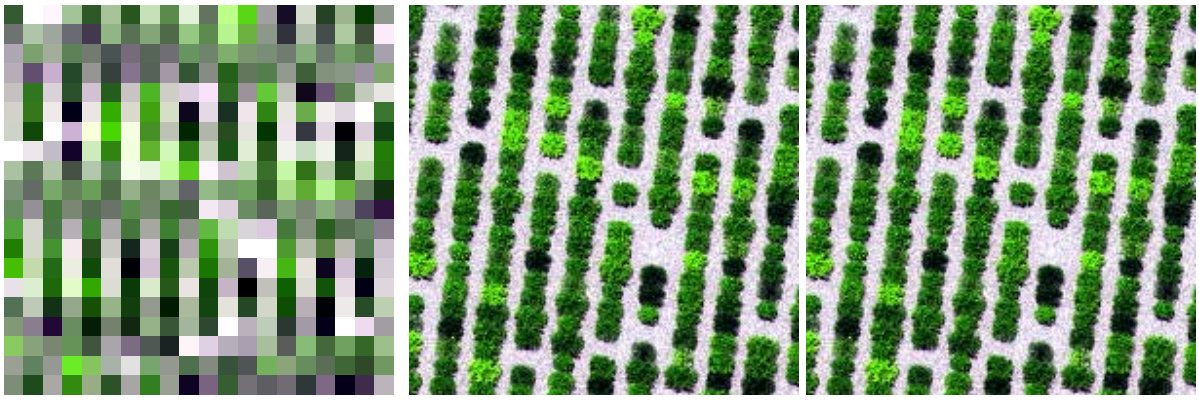

Figure 3: A RGB representation of the synthetic images of the virtual orchard (left:HS – 2m, centre: HR – 0.2m and right: HR-HS – 0.2m) generated using a modified version of a physically based ray-tracer

225 2.2 In-situ dataset

226 *2.2.1 Study area and ground reference measurements*

227 The study area was located in Picassent, in the province of Valencia (Spain, 39.38 N, 0.475 E, altitude 47 m),
228 and the experiment was conducted in a drip irrigated area of 310 ha. Citrus was the predominant cultivated
229 crop, for which, an accurate and pre-visual detection of water stress can be of utmost economic importance
230 for farmers. Orchard design is characterized by large (5-6 m) row spacing and canopy ground cover even in
231 the more vigorous orchard is below 65% of the soil allotted per tree. . Three test orchards were selected based
232 on the large variation in plant water status of the measured trees. A total of 14 trees were used for assessment
233 of midday stem water potential (ψs) determined using a pressure chamber in leaves that were bagged at least
234 1 h prior the measurements. Stem water potential was chosen as the true field determination of citrus trees
235 water status due to its sensitivity to water deprivation (Ballester et al. 2012). The ψs data measured from each
236 tree were related with the individual tree canopy temperature (Tc) extracted from the airborne imagery.
237 Within the selected trees, ψs varied from –0.6 to –2.0 MPa. According to a previous study by Ballester et al.
238 (2012), these values correspond to well watered and relatively severe tree water stress conditions,
239 respectively.

240

241

242 Figure ????

243

244

245

246 *2.2.2 Airborne imagery*

247 Airborne hyperspectral APEX (Airborne Prism Experiment) imagery was acquired over the study area on 8
248 September 2011 around solar noon. The air temperature and VPD at flight time on the date of the flight were
249 30.4 ºC and 2.1 kPa respectively. The APEX recorded the reflectance in 288 bands in the 380 - 2500nm
250 spectral range with spatial resolutions of 2.7 m. The airborne measurements were accompanied with spectral
251 field and lab measurements for calibration and validation of the airborne data. Images were atmospherically
252 and geometrically corrected [3,4,5]. APEX geometric correction was accomplished based on the delivered
253 metadata (i.e. IMU). Atmospheric correction was performed with the in-house processing chain of VITO,
254 based on the algorithms of ATCOR (Biesemans et al., 2007). The geometric correction was performed by
255 VITO's own developed C++ module and is based on direct georeferencing. Input data from the sensor's
256 GPS/IMU, boresight correction data and the SRTM DEM were further used during the geometric correction
257 process. Finally the data were projected to the geographic coordinated system lat/lon, WGS84.

258

259 Another set of aerial images was collected on 23st August 2011 at 10:00 GMT time with a RPAS equipped
260 with a thermal camera, acquiring imagery at 20 cm resolution. Surface temperature was obtained applying
261 atmospheric correction methods based on the MODTRAN radiative transfer model. The mosaicking process
262 selects only the most nadir part of the overlapping images, limiting the viewing angle and thus avoiding
263 directional effects and thermal hotspot. Each snapshot had a relative temperature scale, being the minimum
264 value the coldest pixel and the maximum value the hottest pixel of the snapshot. The air temperature and
265 VPD at flight time on the date of the flight were 31.6 ºC and 1.9 kPa respectively.

Based on the temperature differences between plant canopy and air temperature (Tc-Ta), all background and non-photosynthetic trees were masked. This region of interest was subsequently overlaid on the APEX image to remove all redundant information from the APEX scene. This, however, also implied the removal of all warm, i.e., non transpiring and/ or dead trees.

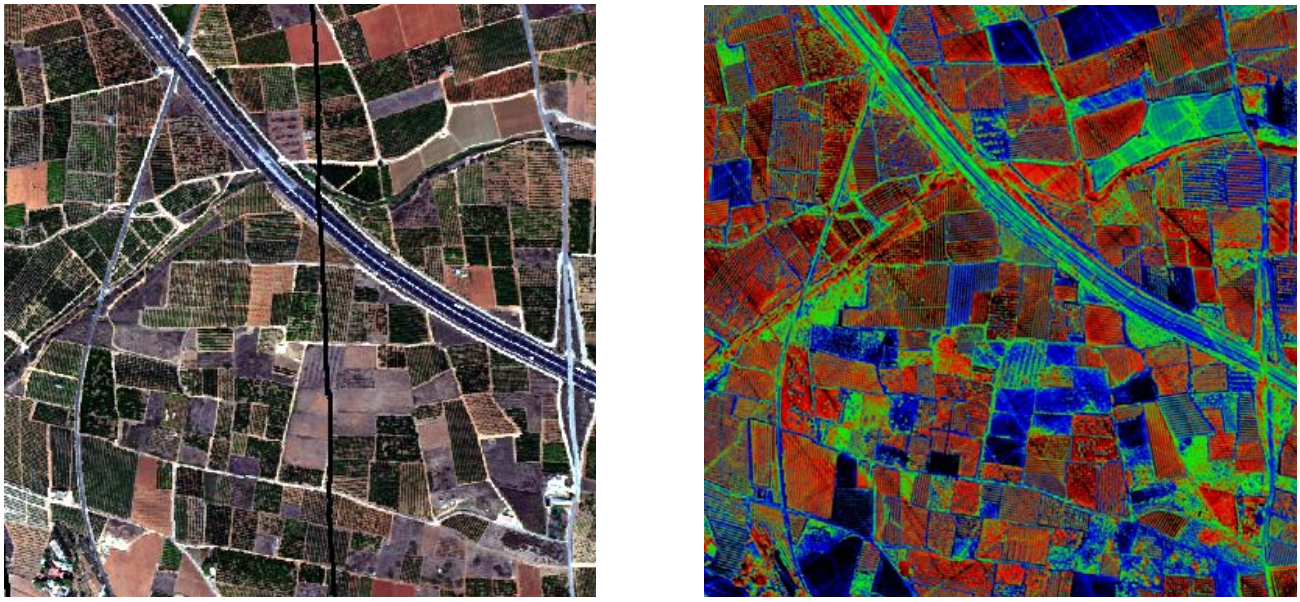

Figure 5: Left: APEX region of interest with 288 spectral bands and 2.80m spatial resolution, Right: RPAS region of interest with 1 thermal band and 0.28m spatial resolution.

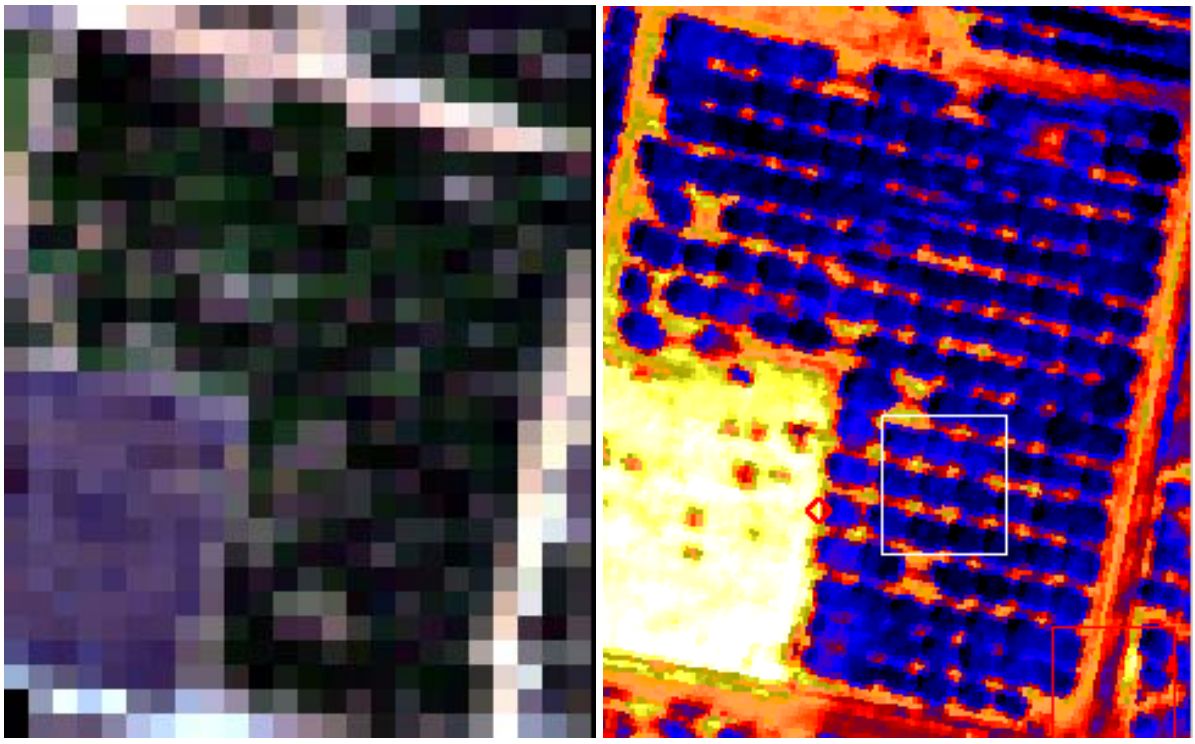

Figure 6: Left: 10x zoom of APEX orchard with 288 spectral bands and 2.80m spatial resolution, Right: RPAS orchard with 1 thermal band and 0.28m spatial resolution.

2.3 Unmixing based fusion of high spectral and high spatial data

The high spectral, low spatial and high spatial, low spectral images obtained from the simulation exercise as well as from the real case study, were fused and analyzed in an automated way in order to obtain a high spatial, high spectral resolution scene (SpU). The only requirements to run the fusion process were the parameterization of the kernel size and the number of classes or endmembers . These parameters had to be carefully thought-out, since they have a vast impact on the reconstruction of the hyperspectral signatures and the endmember variability inherently obtained by the unmixing based fusion processing.

2.3.1 Simulated dataset

For testing the performance of the unmixing based fusion method in estimating biophysical parameter contents, a preliminary study on a fully controlled realistic dataset was performed which allowed managing and creating validation datasets. Since the input parameters were well-known in this simulation exercise, the usefulness of the spatial unmixing techniques on the biophysical parameter extraction on high spatial, high spectral resolution data could be analyzed. We focused on water and chlorophyll content estimation. A robust classification of the high spatial image was achieved by the linear discriminant analysis method with endmember selection as available in the open source ENVI/IDL code (Bertels, 2013). After a sensitivity analysis (results not shown) an optimal kernel size of 5×5 pixels was defined. Changing the kernel size had a major impact on the endmember variability in the scene and played an important role in the reconstruction of the hyperspectral signatures.

Since the data in this experiment was simulated, the portions or fractions of these input parameters for each pixel were known as well. Multiplying these fractions with the leaf water and chlorophyll content values enabled the reconstruction of reference water and chlorophyll maps. Hitherto, two reference biophysical parameter maps and four spectral images, i.e., LR-HS, HR, HR-HS simulated images and the unmixing based fused HR-HS, referred to as SpU image, were available. Subsequently, for the LR-HS, HR-HS and SpU images, standardized difference vegetation index (SDVI) maps were calculated from the spectral reflectance values for each possible combination of two different wavelengths (Delalieux et al., 2008; eq.2).

$$SDVI = \frac{\lambda_i - \lambda_j}{\lambda_i + \lambda_j} \quad (2)$$

with λ_i and λ_j being the spectral reflectance at wavelength *i* and wavelength *j*, respectively, with *i* and *j* ranging from 400-2500 nm.

A coefficients of determination (R^2) index map for each possible SDVI map and the reference water and chlorophyll maps, was then calculated. This approach allowed the selection of an optimal SDVI to estimate water and chlorophyll content and in the mean time allowed to check how well the commonly used biophysical parameter related vegetation indices perform on the (i) high spectral – low spatial (LR-HS), (ii) high spatial-high spectral (HR-HS), and the (iii) fused high spectral-high spatial (SpU) dataset. The R^2 index maps of the LR-HS and SpU images were evaluated based on their correlation with the R^2 maps of all possible SDVI's calculated on the HR-HS simulated reference image.

Next to the assessment of the index performances, the hyperspectral signatures reconstruction through unmixing based fusion were evaluated as well. The Root Mean Square Error (RMSE) and Relative Root Mean Square Error (RRMSE) were calculated to compare the hyperspectral signals from the reference HR-HS image and the modelled signals from the SpU and LR-HS (upscaling with a factor 10) images. RMSE, defined in eq 3, is a measure of the standard deviation, while RRMSE, defined in equation 4, is RMSE as a percentage of the mean observation. RMSE and RRMSE should be as small as possible, optimally zero.

$$RMSE = \sqrt{\sum_{i=1}^{n} \frac{(O_i - P_i)^2}{n}} \tag{3}$$

$$RRMSE = \sqrt{\sum_{i=1}^{n} \frac{(O_i - P_i)^2}{n}} \cdot \frac{1}{\overline{O}} \tag{4}$$

In equations (3) and (4), O_i is the reference or observed value at wavelength i: P_i the predicted value at wavelength i; n the total amount of measurements and $\overline{O}$ the average of the observations.

2.3.2 Real data experiment: Precise water management in fruit orchards

The thermal, high spatial resolution RPAS (section 3.2.4) and high spectral resolution airborne APEX images (section 3.2.3) were used as input in the unmixing based fusion model. The thermal RPAS data was therefore

classified in three temperature classes. A kernel size of 5×5 was defined as most optimal. Combining different kind of images requires a perfect coregistration. 15 ground control points (GCPs) were identified in both images for warping them such that they perfectly fitted each other.

(Jackson et al., 1977b; Idso et al., 1978; Jackson and Pinter, 1981).

Vegetation indices provide a simple and efficient method for extracting water content or estimating water stress from complex canopy spectra. It has to be mentioned that broad waveband vegetation indices typically lack diagnostic capability for identifying certain stress levels. Narrow band indices (Table X) closely related to the (i) epoxidation state of the xanthophylls cycle, (ii) chlorophyll a+b concentration (iii) blue/green/red ratio indices, (iv) carotenoid concentration and (v) tree crown structure have been applied in a previous study to detect water stress in citrus orchards at the tree level (Zarco-Tejada et al., xxx). It was concluded from that study that the xanthophyll pigment related Photochemical Reflectance Index (PRI) calculated with the 570 nm (PRI_{570}) (Gamon et al., 1992) as well as with 515 nm (PRI_{515}) band as a reference (Hernández-Clemente et al., 2011) was significantly related to the stem water potential, and as such indirectly to the water status of the plant. Also in other studies, PRI has been used to assess pre-visual water stress at leaf level (Thenot et al., 2002 and Winkel et al., 2002), at canopy level (Dobrowsky et al., 2005; Evain et al., 2004; Peguero-Pina et al., 2008; Sun et al., 2008) and using airborne imaging spectroscopy (Suárez et al., 2008). The PRI index, (Gamon *et al.*,1992; Peñuelas *et al.*, 1995), is based on the short-term reversible xanthophyll pigment changes accompanying plant stress (Gamon et al., 1990; Peñuelas et al., 1994). These changes are linked to the dissipation of excess absorbed energy that cannot be processed through photosynthesis (Demmig-Adams, 1990, Gamon et al. 1997, Peñuelas and Filella 1998, Peñuelas and Inoue 2000, Trotter et al. 2002). At the leaf and canopy levels, the PRI has been extensively found adequate to estimate photosynthetic performance (Garbulsky *et al.*, 2011).

Also the Transformed Chlorophyll Absorption Ratio Index (TCARI) showed sensitivity to stress levels, and the blue/green ratio BGI1 was highly significant. The effects of water stress on the canopy structure were successfully captured by structural indices such as NDVI, RDVI, SR, MSR, OSAVI, TVI and MTVI. For the 14 trees under investigation in the three selected orchards of the study area, the correlation between all possible SDVIs, including the above-mentioned indices, and the stem water potential was calculated. The index pixel values of the SpU image (28 cm) were averaged over each tree.

As suggested in numerous studies, also temperature profiles of trees (Jackson et al., 1977b; Idso et al., 1978; Jackson and Pinter, 1981) and the stem water potential (Shackel et al. 1997; Naor 2000) are reliable plant-based water status indicators for irrigation scheduling in fruit trees. Therefore, a relationship was sought between the vegetation indices, calculated from the fused and the original APEX datasets, and the in-situ measured stem water potentials as well as between the thermal data and the stem water potentials.

3. RESULTS AND DISCUSSION

3.1 Simulated dataset

The unmixing based fusion of the LR-HS and HR simulated image data resulted in a SpU image containing 216 bands at 20 cm resolution. The added value of the proposed method in estimating water and chlorophyll content is illustrated by calculating the correlation between all possible SDVIs and biochemical parameter reference maps. These reference maps were reconstructed from the fraction images and the C_w and C_{ab} input parameters of PROSPECT, illustrating the water and chlorophyll content variation in the simulated citrus orchard (Figure 7).

For each simulated image, i.e. (i) high spatial, (ii) high spectral, and (iii) high spatial and spectral, the correlation between all possible SDVIs and the reference maps are summarized in Figure 8.

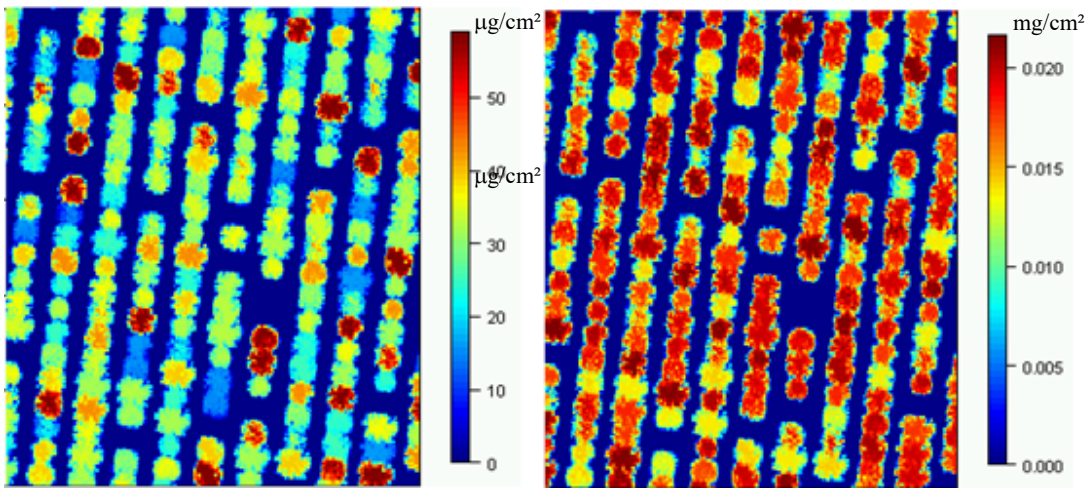

Figure 7: The reference chlorophyll (left) and water map (right)

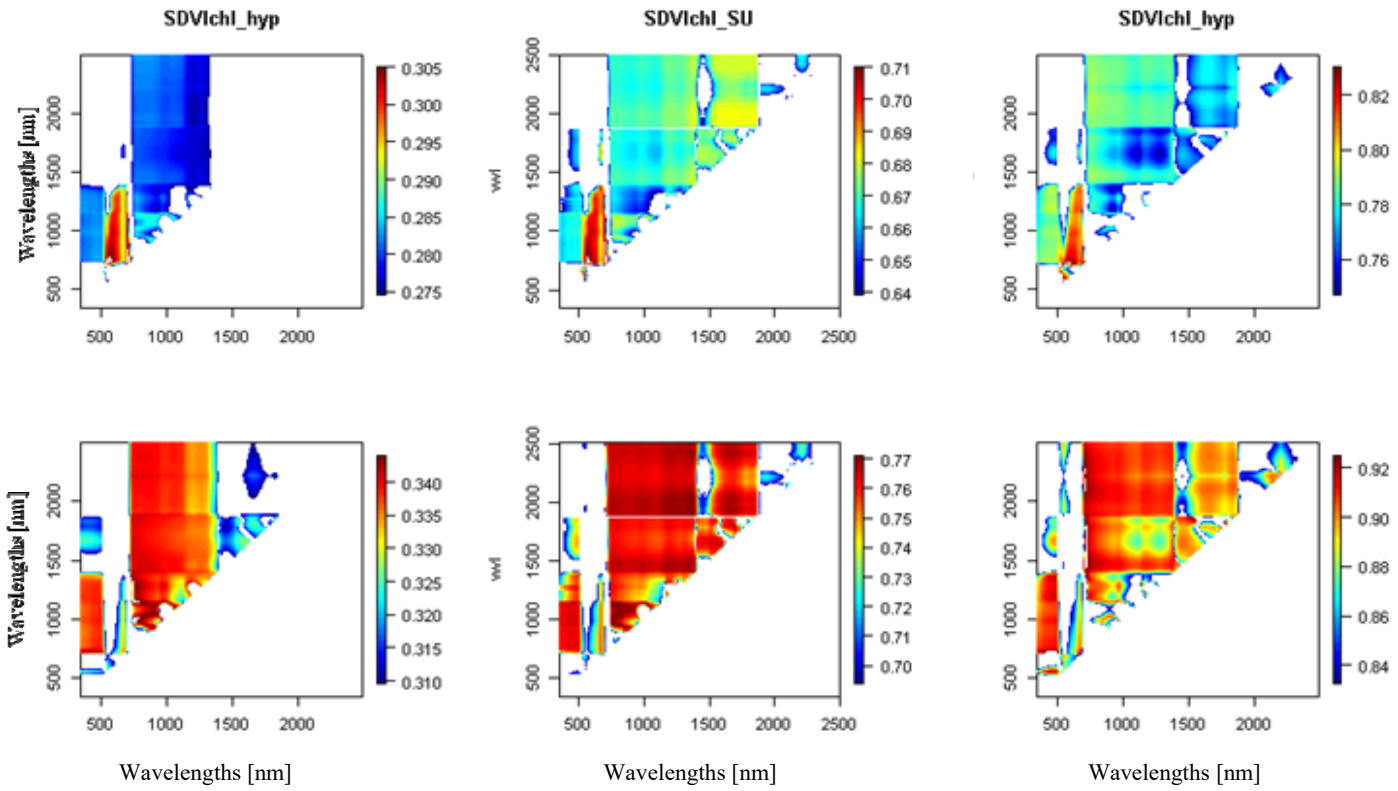

Figure 8: R^2 values indicating the performances of each possible SDVI to estimate chlorophyll (top) and water content (bottom) of the LR-HS, SpU, and HR-HS simulated images. A lower threshold value is defined for each image to enlarge the colour contrast

According to our expectations, the general patterns of the best performing SDVI's were similar throughout the three images with no significant difference in correlations ranging between 73 and 83%. A significant increase in predictive power of the model was found for the SpU algorithm with maximal R^2 values, for the spatially unmixed image (max R^2 = 0.77 for water and 0.71 for chlorophyll), compared to the high spectral, 2 m resolution image (max R^2 = 0.35 and 0.30). As expected, the most appropriate water related indices contain a shortwave infrared (SWIR) waveband corresponding to the highest coefficient of absorption by water as shown in Figure 9. This is also true for the most appropriate chlorophyll related indices, being those containing wavebands with highest absorption coefficients for chlorophyll (620-700 nm).

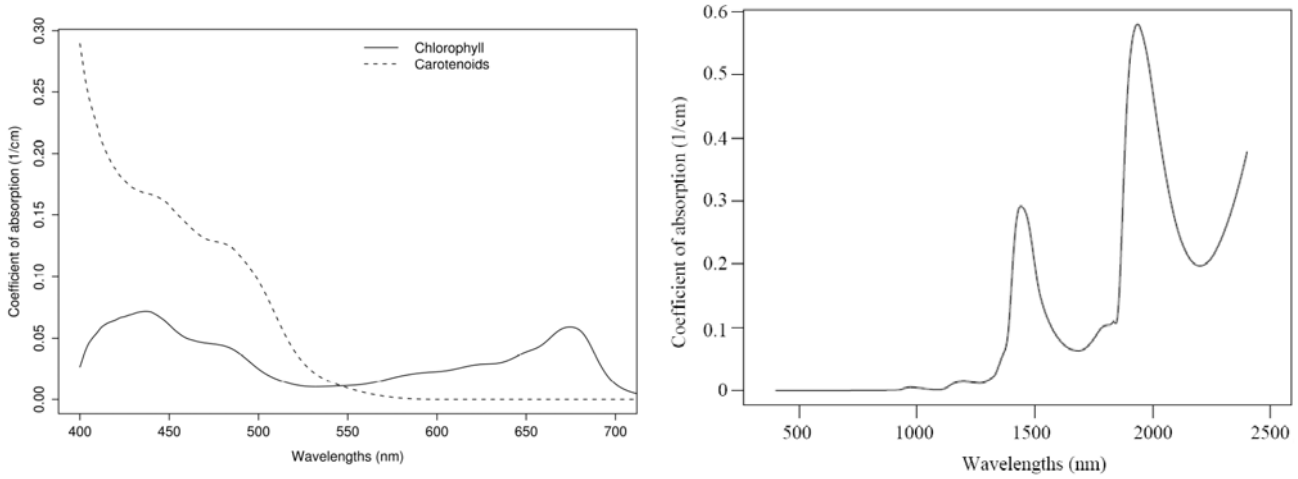

Figure 9 (left): The absorption spectrum of chlorophyll and carotenoids (Absorption characteristics obtained from PROSPECT (Feret et al., 2008) and the LOPEX data set (Hosgood et al., 1994)); (right) The absorption spectrum of water (Absorption characteristics obtained from PROSPECT (Jacquemoud et al., 1996)

The best performing indices (eq. (5) and (6)) to estimate water and chlorophyll content respectively were extracted from these analyses and applied on the three images to provide water and chlorophyll content maps extracted from the information available in the LR-HS, SpU and HS-HR image.

For easy interpretation, also the reference index maps, based on the PROSPECT input parameter are shown (Figures 10 and11).

$$\frac{\lambda_{730} - \lambda_{1510}}{\lambda_{730} + \lambda_{1510}} \quad (5)$$

$$\frac{\lambda_{540} - \lambda_{590}}{\lambda_{540} + \lambda_{590}} \quad (6)$$

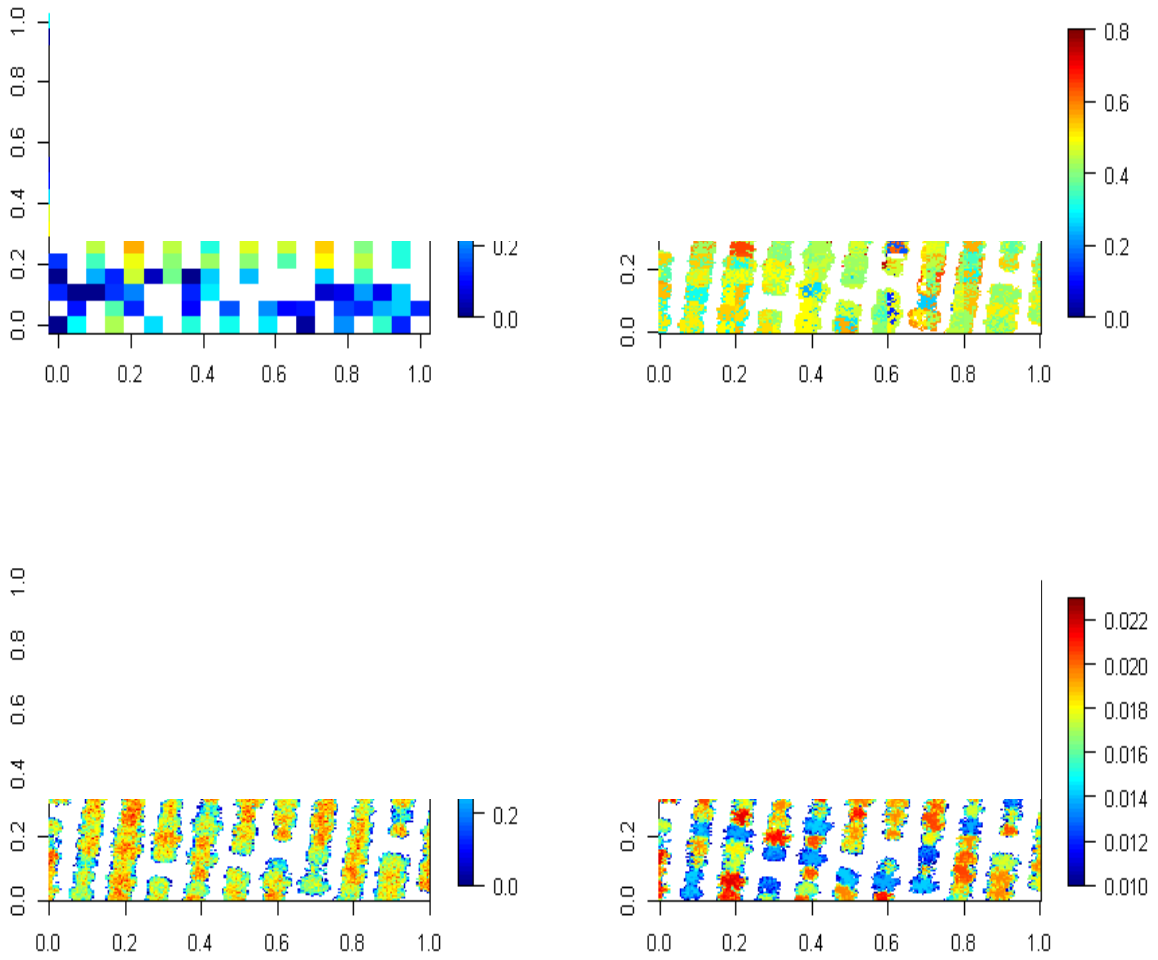

417

418 *Figure 10: Index (eq.5) maps representing water content extracted from the LR-HS (top left), SpU (top right),*

419 *HR-HS (bottom left)images, and reference water content map (bottom right).*

420

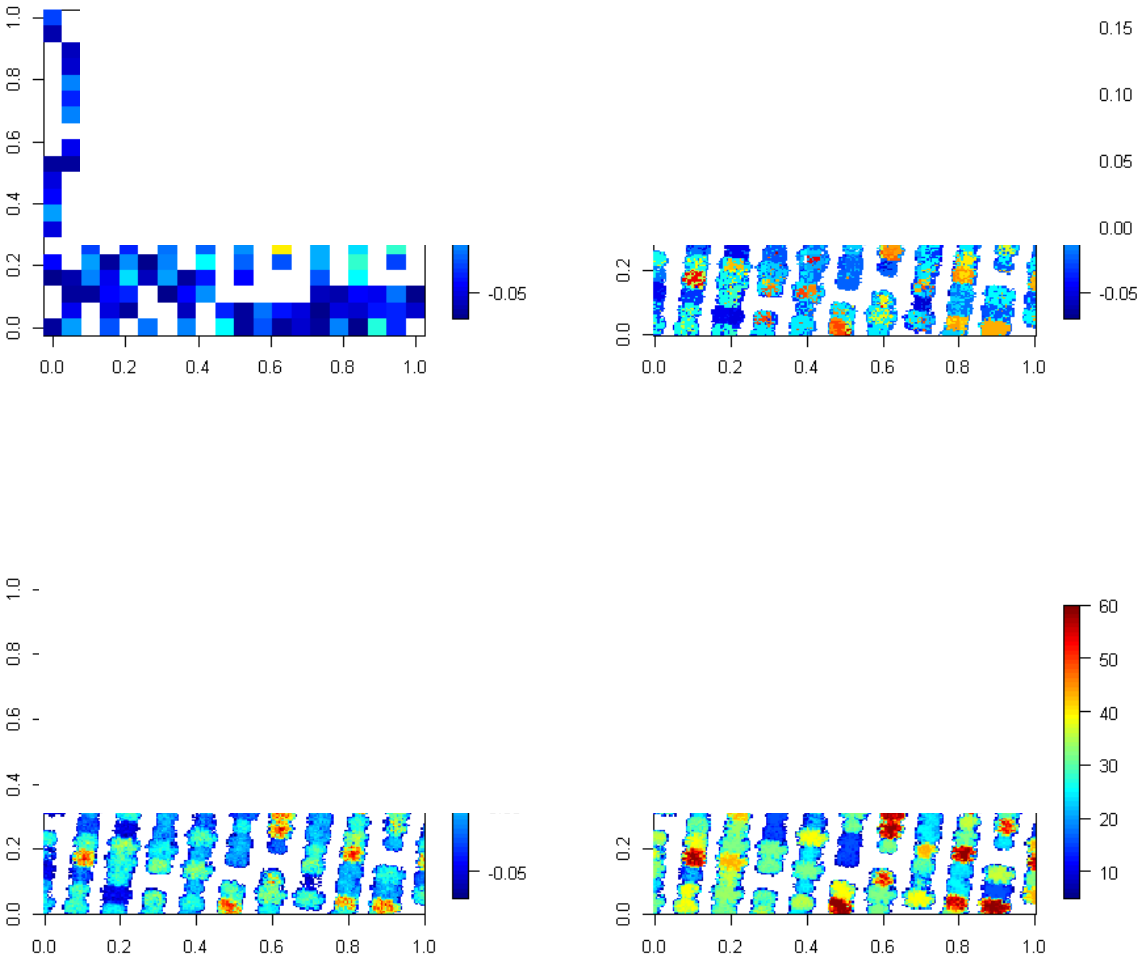

Figure 11: Index (eq.6) maps representing chlorophyll content extracted from the LR-HS (top left), SpU (top right), HR-HS (bottom left)images, and reference chlorophyll content map (bottom right).

We can conclude from Figures 10 and 11 that the spatial resolution of 2.8 m can be beneficial for large scale mapping and monitoring of the citrus orchard, e.g. for delineating management zones in the orchard. However, the resolution is too coarse to precisely manage the orchard system in which an optimisation of yield with a restricted input of natural resources is endeavoured. This corroborated previous results of..... A

high-resolution (temporal and spatial), high-accuracy and low-cost technology in crop and environmental info acquisition is required to provide such a timely information support for agricultural production and accurate and precise management.

The usefulness of the unmixing based fusion technique for detailed stress monitoring is furthermore proven by the general and significant increase in SpU, compared to LR-HS signature, modelling accuracy (Figure 10). Compared to the low resolution spectra, the increase was specifically remarkable in the 350 to 800 nm and 1200 to 2500 nm domain which is most probably due to the higher differences between soil and vegetation spectra in these regions. This indicates that the mixing effects of vegetation and soil spectra which remains the main bottleneck for using LR-HS imagery in precision agriculture (Peddle & Smith, 2005; Stuckens et al., 2010; Tits et al., 2013) is mainly solved by introducing the SpU algorithm. The results of SpU for the extraction of the vegetation signal, as shown in Figure 10, were similar to the MESMA approach in Tits et al.(2013), with RRMSE values between 0.16 and 0.32 for the MESMA approach and between XX and YY for SpU. The correlation with the biophysical parameters after unmixing, however, was higher for SpU, as the correlations obtained with MESMA were only 0.54 and 0.39 for chlorophyll and water, respectively.

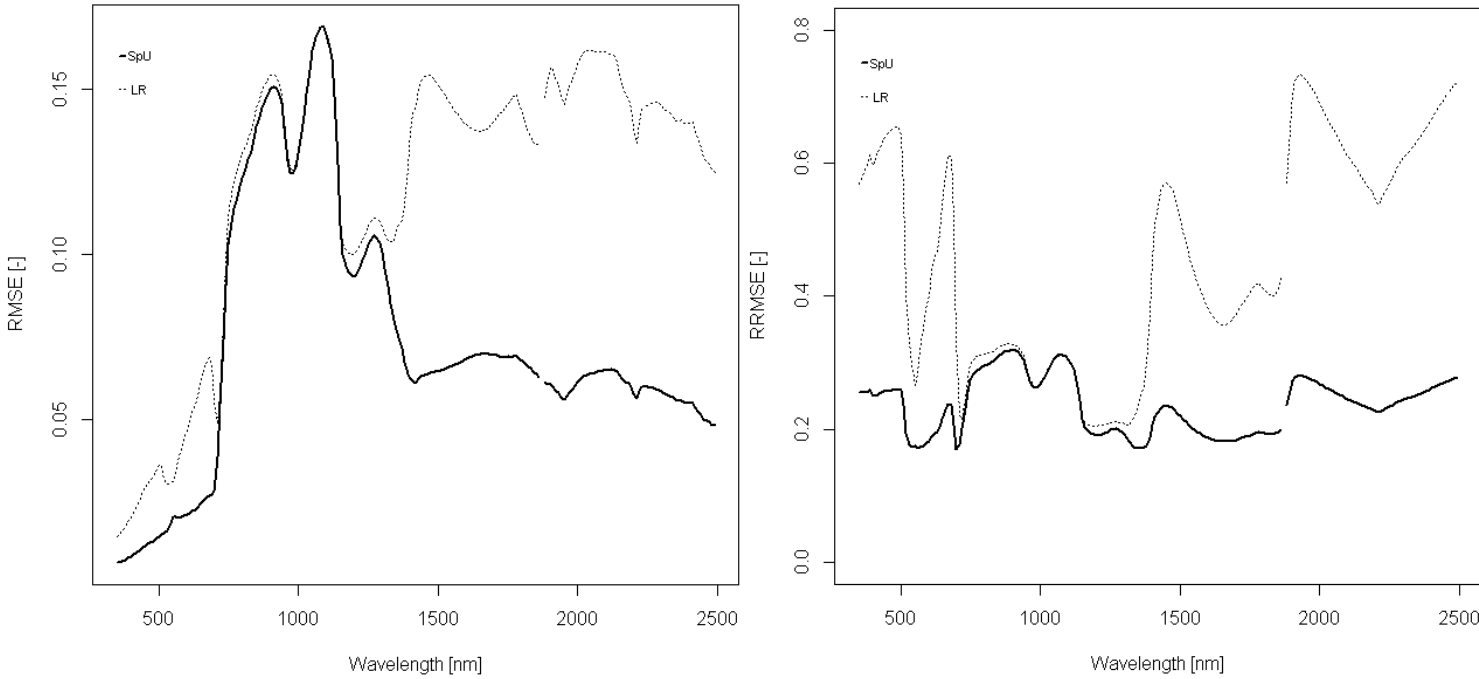

444

445 *Figure 12: RMSE (left) and RRMSE (right) plots calculated from the reference spectra and (i) the*
446 *reconstructed SpU spectra (ii) the downscaled LR-HS spectra.*

447

448 Based on the high correlations between the SDVI performances calculated from the SpU image and those
449 calculated from the reference images, and the high R^2 values of the SDVI biophysical parameter content
450 relations compared to those of the LR image, we may conclude that the SpU method has potential for more
451 detailed research in water and chlorophyll content estimation. Furthermore, the implementation of the
452 unmixing based fusion method seems to provide an opportunity to enhance the orchard management
453 efficiency through the detailed identification of the biochemical parameter contents within the trees. In the
454 following section, the SpU method is used to early detect water stress in a commercial citrus orchard in
455 Spain.

456

457 3.2. In situ dataset

458 Applying the spatial unmixing technique on the 0.28m thermal RPAS and the 2.8m hyperspectral APEX
459 datasets resulted in a spatially unmixed (SpU) image providing 288 bands at 0.28m spatial resolution (Figure
460 13).

461

462 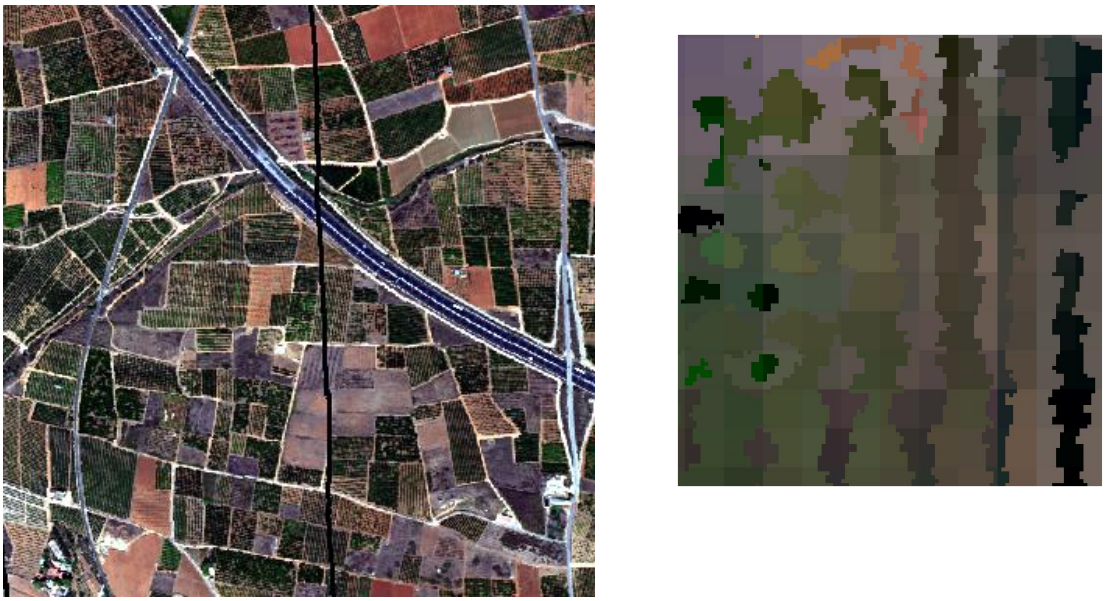
463
464
465
466
467
468
469

470 *Figure 13: SpU image and detailed view*

471

472 Mixing of soils and vegetation in an APEX pixel became already obvious by visually comparing the spectra.
473 The added value of the high spatial resolution lies herein that vegetation indices can be applied on pure
474 vegetation pixels without the contribution of soil background and structural effects.
475 For the 14 trees under investigation in the three selected orchards of the study area, the correlation between
476 all possible SDVIs and the stem water potential is represented in Fig 14, with colour bars indicating the R^2
477 values of the linear relationship between the two parameters.

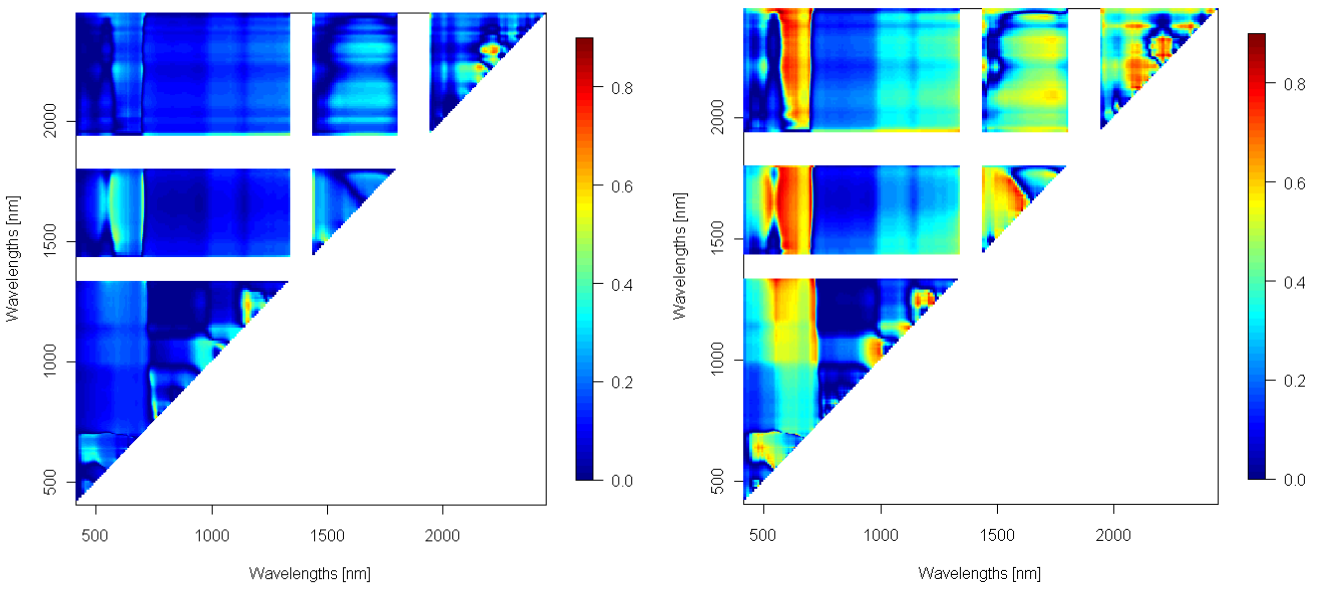

Figure 14: R^2 values of the linear relation between the stem water potential of the 14 trees of interest and all possible SDVIs (left) calculated from APEX pixels (right) calculated from SpU pixels

It is unambiguous that a higher correlation between SDVIs and stem water potential was obtained by applying the SpU algorithm. This is further illustrated by extracting the 21 narrow-band stress-related vegetation indices described in a similar case study performed by Zarco-Tejada et al. (2012). In that study, the authors obtained hyperspectral VNIR images from a RPAS platform from which they calculated the narrow-band indices to relate them with the stem water potentials for water stress detection in citrus orchards. A comparison of the coefficients of determination obtained through narrow-band indices from APEX and SpU imagery against stem potential is shown in Table 1. Similar trends were found in the relation between vegetation indices obtained from APEX tree pixels and stem water potential compared to those obtained from SpU tree pixels. However, an overall better relationship has been found for the SpU pixels, particularly for the PRI570 index (Figure 15). This pre-visual stress indicator is definitely more related to stem water

492 potential or water stress when the SpU method is applied as shown in Fig. 15 and Table 1. Significant
493 relationships ($p<0.05$) are shown in bold in Figure 15.
494
495 The most appropriate SDVIs to estimate water content obtained from the simulation study (Figure 8) and the
496 SDVIs which were most related to stem water potential (Figure 14) differed mostly from each other in those
497 containing NIR bands. This corresponds to the spectral region mainly controlled by leaf and canopy
498 structural parameters having the highest RMSE and RRMSE scores for the unmixing based fusion method
499 (Figure 12).
500
501 **Table 1: Coefficients of determination R^2 obtained through narrow-band indices from APEX and SpU imagery against**
502 **stem potential.**

	SpU - ψ	APEX - ψ
PRI570	0.62 ***	0.21
BRI2	0.47 **	0.29*
R_{515}/R_{570}	0.42 *	0.16
R_{515}/R_{670}	0.38 *	0.14
ZM	0.35 *	0.12
OSAVI	0.34 *	0.05
G	0.34 *	0.14
NDVI	0.34 *	0.13
SR	0.34 *	0.13
MSR	0.34 *	0.12
VOG1	0.31 *	0.09
PRI515	0.24	0.09
R_{520}/R_{500}	0.23	0.05
TCARI	0.14	0.02
RDVI	0.13	0.02
BGI1	0.12	0.01
LIC3	0.12	0.06
TVI	0.09	0.01
MTVI	0.09	0.00
BGI2	0.02	0.00
BRI1	0.01	0.01

* p<0.05

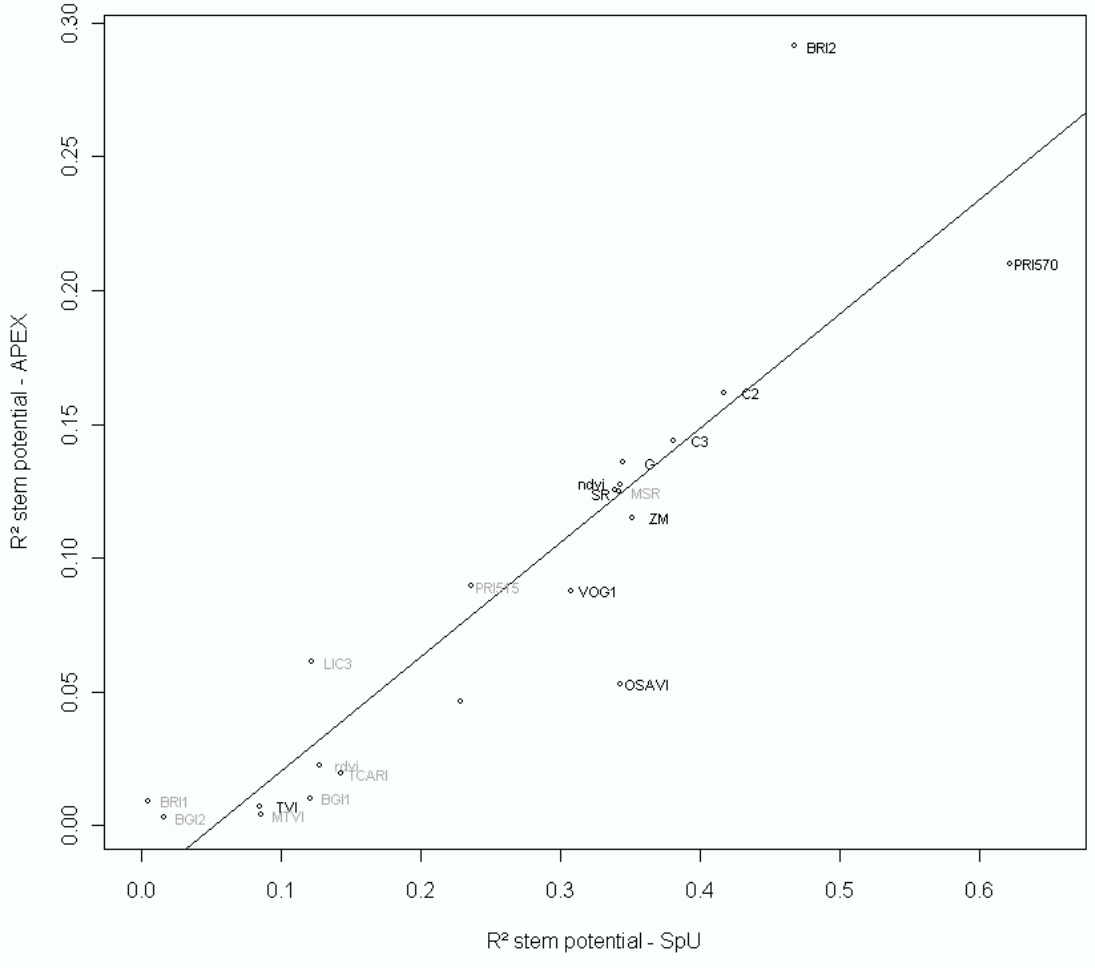

** p<0.01
*** p<0.001

Figure 15: Representation of the correlation between the coefficients of determination R^2 obtained through narrow-band indices from APEX and SpU imagery against stem potential.

As can be concluded from Figure 15 and 16, structural and background effects (present in the APEX pixels) have an impact on the PRI values and consequently also on the performance of the PRI to estimate water stress. This is in corroboration with the findings of (refs, Suarez?) who tested the influence of structural effects on PRI. Knowing that the stem water potential is a good and reliable estimator of plant water stress, it can be concluded from the relationship shown in Figure 16 that detailed spatial information is vital in water stress detection studies. Significant higher relationships between stem water potential and PRI values were obtained for SpU images ($R^2 = 0.62$) compared to those obtained by the LR-HS APEX image (R^2=0.21).

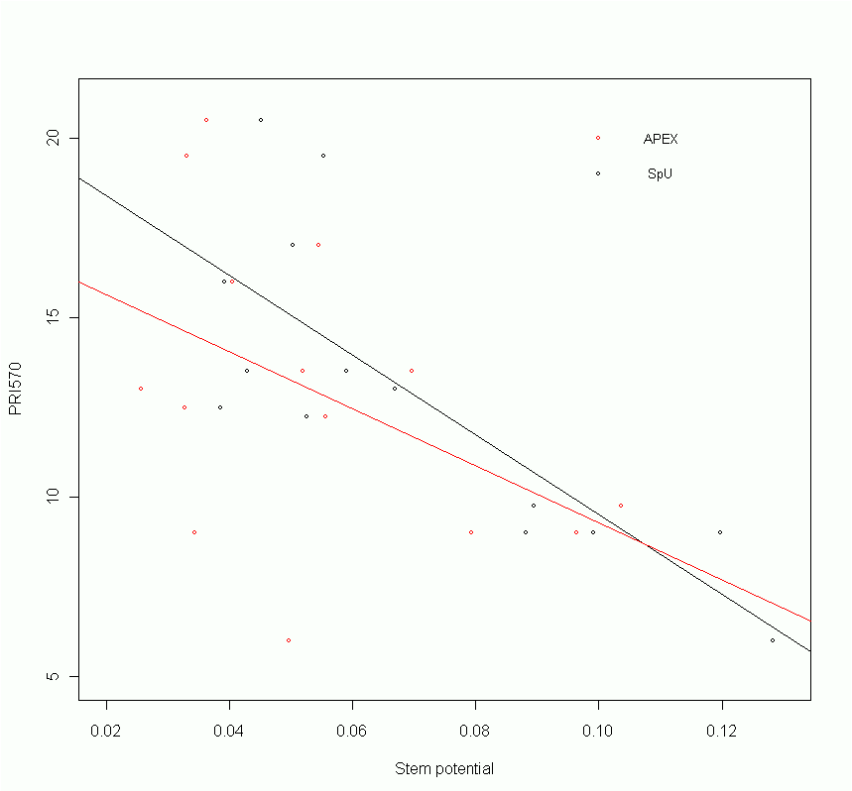

Figure 16: Comparison of APEX (red) and SpU (black) PRI index values correlated to stem potential

Due to the presence or admixture of soil, background and vegetation in the larger APEX pixels, all indices performed worse in estimating water stress in this LR-HS image.

The images shown in Figure 14 indicate that even a better water stress detection should be possible when also the reflectance patterns of the SWIR domain could be captured by the sensor. Numerous previous remote sensing studies have proven that the spectral behaviour of vegetation in the SWIR spectral domain is severely influenced and masked by water absorption. In this study, R^2 values up to 0.81 were obtained through a linear relation of SpU derived SDVIs based on 562 and 1650 nm against stem water potential. The reflectance absorptions in the 1650–1850 nm region are known to reflect not only the leaf water content, but also the contents of leaf cellulose and lignin, and are directly related to the plant growing status (Curran 1989, Zagolski 1996). Moreover, the 1650–1850nm band combines an excellent soil-green vegetation spectral contrast with within band sensitivity to the leaf water content and the influence of the atmosphere on solar irradiance is small (Gausman 1978, Valley 1965).

However, current technology does not yet allow to gather such a high spatial, high spectral imagery over the full spectral range with airborne sensors. By fusing high spatial and high spectral images a new data source is created which opens new and promising opportunities for e.g., detailed water stress mapping. At the ground level, stem water potential (ψs) is known to be a reliable plant-based water status indicator for irrigation scheduling in fruit trees (Shackel et al. 1997; Naor 2000). However, its measurement is a cumbersome procedure and requires frequent trips to the field and a significant input of labour. In addition, because plant water status varies is dynamic during the course of the day, only a few measurements can be performed what limits the determination of plant water status to a few orchards at a time. For these reasons, efficient and non-destructive methods looking beyond the visual spectral range, for the detection of water stress' induced plant

physiological changes were searched for to better steer the citrus water management system. In addition, the possibility of determining plant water status in large areas expand the possibilities of using remote sensing detection of plant water status beyond the farm level, increasing the opportunities for commercial applications of the developed technology.

From previous studies (Cohen et al., 2005; Idso et al.,1978; 1981; Jackson et al., 1977, 1981; Jackson & Pinter, 1981; Leinonen & Jones, 2004; Möller et al., 2007; Sepulcre-Cantó et al., 2006, 2007; Wanjura et al., 2004), we know that a good correlation should exist between thermal data and water stress or stem potentials, which was not found in our study, due to a miscalibration of the thermal sensor. Within one image, the relation between stem potentials and thermal data was high (R^2=0.72), but not as high as the PRI calculated from the SpU and water potentials relation (R^2=0.80) within that same image. The temperature differences caused by the sensor were masked in the fusion method due to its inherent characteristic to reconstruct hyperspectral endmember signatures based on the materials present in the pixels within the kernel.

4. CONCLUSION

The aim of the study was to apply an unmixing based fusion technique on a hyperspectral APEX and hyperspatial RPAS dataset for a better assessment of biophysical parameters in agricultural areas. We first tested the unmixing based fusion method on simulated datasets to evaluate the proposed method through standardized vegetation indices and spectral signature reconstruction. Based on the high correlations between the SDVI performances calculated from the SpU image and those calculated from the reference images, and the high R^2 values of the SDVI biophysical parameter content relations compared to those of the LR image,

561 we concluded that the SpU method has a lot of potential for more detailed research in water and chlorophyll
562 content estimation.
563 Subsequently, the fusion method was applied on a real test case, in which hyperspectral APEX and
564 hyperspatial thermal RPAS images were combined in order to better and more accurately detect water stress
565 in commercial citrus orchards. Assuming that the stem water potential and PRI index are good indicators of
566 water stress levels, it can be decided that a higher spatial resolution (SpU) image obtained from fusing high
567 spatial thermal RPAS images and high spectral APEX images, is better suited (R^2=0.62 vs 0.21) for detailed
568 water stress estimation.
569 This fusion technique offers new opportunities to the user community in that higher spatial spectral
570 dataset become available for their research or operations. The need for a perfect co-registration of the two
571 input images (i.e., high spatial and high spectral) can be seen as the major drawback of this technique. A lot
572 of effort has to be put in this processing step, which has a large impact on the resulting fused image if not
573 carefully done. Ideally, the two sensors, of which one is focused on the spatial detail and the other focused on
574 the spectral detail should be mounted on one chip, so that coregistration is not an issue anymore.
575
576 ACKNOWLEDGEMENTS
577 We thankfully acknowledge that this research received funding from the Belgian Science Policy Office in the
578 frame of the Stereo II programme (Hypermix project - SR/00/141). Hyperstress EUFAR
579
580 REFERENCES
581
582 Bertels, L., 2013. http://sourceforge.net/projects/enviidlcodelibr/files/

583 Ballester, C., Castel, J., Intrigliolo, D.S., Castel, J.R., 2011. Response of Clementina de Nules citrus trees to
584 summer deficit irrigation. Yield components and fruit composition. Agricultural Water Managent 98, 1027-
585 1032.
586 [1] D. Filiberti. "Combined spatial-spectral processing of multisource data using thematic content." A
587 Dissertation Submitted to the Faculty of the department of electrical and computer engineering. In Partial
588 Fulfillment of the Requirements for the Degree of doctor of Philosophy. The University of Arizona, pp. 119,
589 2005.
590 [2] R. Zurita-Milla, J.G.P.W. Clevers, M.E. Schaepman. "Unmixing-based Landsat TM and MERIS FR Data Fusion." *IEEE*
591 *Geoscience and Remote Sensing Letters*, 5, pp. 453-457, 2008.
592 [3] J.A.J. Berni, P.J. Zarco-Tejada, L. Suarez, and E. Fereres, "Thermal and Narrow-band Multispectral
593 Remote Sensing for Vegetation Monitoring from an Unmanned Aerial Vehicle." *IEEE Transactions on*
594 *Geoscience and Remote Sensing*, 47, (3), pp. 722-738.
595 [4] J. Biesemans, S. Sterckx, E. Knaeps, K. Vreys, S. Adriaensen, J. Hooyberghs, K. Meuleman, P. Kempeneers, B. Deronde, J.
596 Everaerts, D. Schläpfer, and J. Nieke, "Image processing workflows for airborne remote sensing." *Proceedings of the 5th EARSEL*
597 *Workshop on Imaging Spectroscopy*, Bruges, Belgium, April 23-25 2007.
598 [5] J.A. Sobrino, J.C. Jiménez-Muñoz,, P.J. Zarco-Tejada, G. Sepulcre-Cantó, and E. de Miguel, "Land Surface Temperature
599 derived from Airborne Hyperspectral Scanner Thermal Infrared data." *Remote Sensing of Environment*, 102, 99-115.
600 [6] J. Gamon, J. Penuelas, and C.B. Field (1992). "A narrow-waveband spectral index that tracks diurnal
601 changes in photosynthetic efficiency." *Remote Sensing of environment*, 41, 35-44.
602 [7] L. Suárez, P.J. Zarco-Tejada, G. Sepulcre-Cantó, O. Pérez-Priego, J.R. Miller, J.C. Jiménez-Muñoz, and
603 J. Sobrino (2008), "Assessing canopy PRI for water stress detection with diurnal airborne imagery" *Remote*
604 *Sensing of Environment,* 112, 560–575
605 B. Somers, S. Delalieux, W. W. Verstraeten, and P. Coppin, "A conceptual framework for the simultaneous extraction of sub-pixel spatial
606 extent and spectral characteristics of crops," *Photogramm. Eng. Remote Sens.*, vol. 75, pp. 57–68, 2009

Pharr M, Humphreys G. Physically based rendering. From theory to implementation. San Fransisco: Morgan Kaufmann; 2004.

J. Chavez, Pat S., S. C. Sides, and J. A. Anderson, "Comparison of three different methods to merge multiresolution and multispectral data: Landsat TM and SPOT panchromatic," *Photogrammetric Engineering and Remote Sensing*, vol. 57, no. 3, pp. 295–303, 1991.

T. Guo, T. Kujirai, T. Watanabe (2012) Mapping crop status from an unmanned aerial vehicle for precision agriculture applications. International Archives of the Photogrammetry, Remote Sensing and Spatial Information Sciences, Volume XXXIX-B1, 2012. XXII ISPRS Congress, 25 August – 01 September 2012, Melbourne, Australia

Weber J, Penn J. Creation and rendering of realistic trees. In: Proceedings of the Siggraph, 1995.

Peddle DR, Smith, M. (2005). Spectral mixture analysis of agricultural crops : endmember validation and biophysical estimation in potato plots. International Journal of Remote Sensing, 26, 4959-4979

Stuckens, J., **Somers, B.**, Dzikiti, S., Verstraeten, W.W., Albrigo, G., Swennen, R., Coppin, P. (**2010**). Off-nadir viewing and sensor specifications for reducing spectral mixture issues in Citrus orchards. Photogrammetric Engineering and Remote Sensing, 76, 1261-1274

Tits, L., **Somers, B.**, Stuckens, J., Farifteh, J., Coppin, P. (**2013**). Integration of in situ measured soil status and remotely sensed hyperspectral data to improve plant production system monitoring: concept, perspectives and limitations. Remote Sensing of Environment, 128, 197-211

int. j. remote sensing, 2001, vol. 22, no. 12, 2329–2338

Spectroscopic determination of wheat water status using

1650–1850 nm spectral absorption features
Q. TIAN, Q. TONG, R. PU

1. Tits, L., **Somers, B.**, Stuckens, J., Farifteh, J., Coppin, P. (**2013**). Integration of in situ measured soil status and remotely sensed hyperspectral data to improve plant production system monitoring: concept, perspectives and limitations. *Remote Sensing of Environment*, 128, 197-211.
2. Tits, L., **Somers, B.**, Coppin, P. **(2012)**. The potential and limitations of a clustering approach for the improved efficiency of Multiple Endmember Spectral Mixture Analysis in plant production system monitoring. IEEE Transactions on Geoscience and Remote Sensing, 50, 2273-2286

Roberts, DA. (1991) Separating spectral mixtures of vegetation and soil. University of Washington, PhD dissertation, 180 pp.

Somers, B., Cools, K., Delalieux, S., Stuckens, J., Van der Zande, D., Verstraeten, W.W., and Coppin P. **(2009)**. Nonlinear Hyperspectral Mixture Analysis for tree cover estimates in orchards. Remote Sensing of Environment, 113, 1183 – 1193

NONLINEAR SPECTRAL MIXING MODELS FOR VEGETATIVE AND SOIL SURFACES

Author(s): BOREL, CC; GERSTL, SAW
Source: REMOTE SENSING OF ENVIRONMENT Volume: **47** Issue: **3** Pages: **403-416** DOI: **10.1016/0034-4257(94)90107-4**
Published: **MAR 1994**
Times Cited: **137** (from Web of Science)

Widlowski, J. -L., Robustelli, M., Disney, M., Gastellu-Etchegorry, J. -P., Lavergne, T., Lewis, P., et al. (2008). The RAMI on-line model checker (ROMC): A web-based benchmarking facility for canopy reflectance models. Remote Sensing of Environment, 112, 1144–1150.

Tits, L., De Keersmaecker, W., **Somers, B.**, Asner, G.P., Farifteh, J., Coppin, P. **(2012b)**. Hyperspectral shape-based unmixing to improve intra- and interclass variability for forest and agro-ecosystem monitoring. ISPRS Journal of Photogrammetry and Remote Sensing, 74, 163-174